

Photoconductivity in nanocrystalline GaN and amorphous GaON

A. Koo,^{a)} F. Budde, B. J. Ruck, and H. J. Trodahl*MacDiarmid Institute for Advanced Materials and Nanotechnology, School of Chemical and Physical Sciences, Victoria University of Wellington, P.O. Box 600, Wellington, New Zealand*

A. Bittar and A. Preston

Measurement Standards Laboratory, Industrial Research Ltd., P.O. Box 31310, Wellington, New Zealand

A. Zeinert

Laboratoire de Physique de la Matière Condensée, Université de Picardie Jules Verne, F-80039 Amiens Cedex, France

(Received 24 May 2005; accepted 15 December 2005; published online 13 February 2006)

In this work we present a study of the optoelectronic properties of nanocrystalline GaN (nc-GaN) and amorphous GaON (*a*-GaON) grown by ion-assisted deposition. The two classes of film show very distinct photoconductive responses; the nc-GaN has a fast small response while the *a*-GaON films have a much larger response which is persistent. To describe the observed intensity, wavelength, and temperature dependence of the photoconductivity in each class of film, we build a model which takes into account the role of a large density of localized states in the gap. The photoconductivity measurements are supplemented by thermally stimulated conductivity, measurement of the absorption coefficient, and determination of the Fermi level. Using the model to aid our interpretation of this data set, we are able to characterize the density of states in the gap for the two materials. © 2006 American Institute of Physics. [DOI: 10.1063/1.2170400]

I. INTRODUCTION

The fifteen years following the work of Nakamura and Fasol¹ has seen an explosion of interest in devices based on GaN and its alloys. To date these studies and devices are based almost exclusively on epitaxial crystalline films, although the optoelectronic properties are known to have a very high tolerance to grain-boundary defects. In that context it is interesting to note that even polycrystalline GaN has recently been shown to be capable of blue light emission.² A greater interest is therefore developing in the more disordered forms of GaN, both nanocrystalline and amorphous. A thorough theoretical treatment of amorphous GaN has been carried out using *ab initio* molecular dynamics.^{3,4} Not only was stoichiometric, amorphous GaN predicted to be a structurally feasible material but the model also found no deep gap states in spite of the highly defective nature of the structure. The potential of fabricating a visible blind UV detector therefore motivates our investigation of the disordered forms of GaN.

We have developed an ion-assisted deposition (IAD) procedure for the growth of GaN, and optimized the deposition parameters to ensure a 1:1 Ga:N stoichiometry.^{5,6} The films consist of typically 3 nm diameter random-stacked crystallites. They can be stabilized into an amorphous form during growth⁷ by incorporating at least 12 at. % of O, which is accomplished by depositing in the presence of a carefully controlled partial pressure of water vapor. Films have been prepared on a variety of substrates, including glass, fused silica, silicon, and even metals, and there appears to be no significant substrate dependence of the films' properties. In this paper we report the optoelectronic properties of the two

types of film, nanocrystalline GaN (nc-GaN) and amorphous GaON (*a*-GaON), investigated by optical-absorption and photoconductivity (PC) measurements. The nc-GaN is stoichiometric with a Ga:N ratio of unity, and the *a*-GaON to be discussed here has a Ga:(O+N) ratio of unity with an oxygen concentration of either 12 at. % (films GaON-1 and GaON-2) or 24 at. % (film GaON-3).

II. EXPERIMENTAL DETAILS

The preparation and extensive characterization of the films have been discussed in earlier papers,⁶⁻⁹ so here we focus exclusively on the measurements that establish their optical and photoconductive properties. For these measurements we have used typically 200-nm-thick films deposited on fused silica substrates. Turning first to the optical measurements we have determined the reflection and transmission of the film-substrate sample and fitted the results including coherent multiple reflections from the film's surfaces. For this purpose film thicknesses were set near a thickness determined by Rutherford backscattering spectroscopy, and then allowed to vary about that value in order to improve the fit. These reflection/transmission measurements permitted the determination of the absorption coefficients in the range of 10^3 – 10^5 cm⁻¹, for which the absorptive loss in a 200-nm-thick film is in the range of 1%–95% of the incident power. A full characterization of the states within the gap required an extension to much smaller absorption coefficients, for which we have used photothermal deflection spectroscopy.¹⁰

For electrical measurements, an interdigitated pattern of Ohmic Ti/Al electrical contacts¹¹⁻¹³ was formed in order to limit the impedance of the highly resistive films. The pattern gave 50 μm gaps between the fingers with an effective

^{a)}Electronic mail: annette.koo@csiro.au

length of the electrodes of 25 mm and a form factor L/A of 10^2 cm^{-1} . To reduce leakage currents and limit the current noise to 10 fA, special shielding and guarding techniques had to be used. Even with this setup the room-temperature dark resistance of the most resistive films exceeded the measurement limit of $10^{14} \Omega$ under a 9 V bias.

Photoconductivity measurements were made as a function of time, temperature, wavelength, and intensity of the incident light. The source was a Xe arc lamp with a Jobin-Yvon D10 double monochromator, fitted with a grating blazed for the UV. With slits of 2 mm the monochromator passed a bandwidth of 8 nm which then overfilled the sample with a power of approximately 10^{-5} W at each of the wavelengths used, of which about 8% fell on the bare film between the contacts. The power level was measured using a calibrated Si photodiode and a fused silica beam splitter. These arc lamp studies were complemented by intensity-dependent measurements using a 325 nm He/Cd laser passed through various neutral density filters and focused to a spot whose diameter just exceeded the $50 \mu\text{m}$ between electrodes. The intensity range used for this experiment produced a similar current to that achieved in the arc lamp studies wherein the spot overfilled the pattern (a few nanoamperes in the GaON films and even less than a picoampere in the nc-GaN film).

Some of the films display very long lived persistent photoconductivity (PPC) associated with carrier traps in the gap. The PPC required many days to decay so that it was necessary to employ a heated stage to permit a low-temperature anneal to return the films more quickly to their dark conductivity. It will be discussed and exploited below that the release of carriers during an anneal also permits an estimate of the energy dependence of the trap depth distribution. Furthermore, the temperature dependence during the sample cooling allowed a determination of the depth of the Fermi level in the dark configuration. We have reported earlier¹⁴ that these films show structural changes for anneals above $400 \text{ }^\circ\text{C}$; so for the present purpose we have limited the annealing temperatures to $200 \text{ }^\circ\text{C}$.

III. PHOTOCONDUCTIVITY IN DISORDERED SEMICONDUCTORS

Covalent materials, even in a strongly disordered configuration such as those reported here, can have a clear gap between valence and conduction bands. However, they commonly have a significant density of localized carrier states between the bands of extended states, inside what is called the mobility gap. These gap states are of paramount importance to understand the photoconductivity of the films on which we report here. In this section we present a general description of PC in a material which contains these tails of localized in-gap states. The models discussed here will provide a clear understanding of the influence of the gap states and aid the interpretation of the experimental results.

Under illumination, photoexcited carriers at the band edges are rapidly trapped in the tail (trap) states, and the interplay of trapping, thermal detrapping, and recombination from extended states and/or tail states ultimately determines the behavior of the photoconductivity. Under the intensity

and temperature regimes in the present study the density of trapped carriers is many times larger than the density of free carriers. Furthermore, it is unlikely that the two carrier signs, holes and electrons, have similar trapping and detrapping kinetics, so that there will be a large excess of one carrier class in extended states. We arbitrarily describe that majority carrier as electrons, though the obvious symmetry permits the description to be applied equally well if hole conduction dominates. Within this assumption of majority electron carriers the holes become permanently trapped and these then form the recombination centers for electrons in the conduction band. We now distinguish between two cases, depending on whether the recombination takes place from extended or localized (i.e., trap) electron states.

In the first case the electrons are repeatedly trapped and detrapped before recombination from an extended state, so that the distribution of trapped carriers can be described with a quasi-Fermi-level determined by the total number of electrons in the excited (i.e., conduction band plus conduction-band tail) states (see the Appendix). The number of free electrons is then

$$n_c \propto \sqrt{G \exp(-E_t/kT)}, \quad (1)$$

where T is the temperature, G is the generation rate, and E_t is the depth of the quasi-Fermi-level below the conduction-band mobility edge. The generation rate is linear in intensity and absorption coefficient (for our films in which the absorption coefficient is $<1/d$ where d is the thickness of the film).¹⁵ This scenario predicts that the steady-state photoconductivity should have a square-root dependence on the intensity and absorption coefficient, and Arrhenius behavior as a function of temperature. In this case the time dependence of the photoconductivity will be slow: the rise curve reflecting the process of achieving quasithermal equilibrium and the decay after cessation of illumination the process of slowly stripping away the trapped carriers from the top of the distribution of trapped carriers (PPC).

The second case identified is the one in which recombination between trapped carriers occurs not via the conduction band but directly via thermalization, i.e., thermal relaxation of carriers down through localized states to the Fermi level where they recombine. In this case the recombination time is constant as the density of recombination centers is independent of illumination (see the Appendix). The steady-state photoconductivity is therefore linear in generation rate (and hence in intensity and absorption coefficient). The time dependence in this case is expected to be faster than in the previous case since there is no barrier to recombination.

IV. RESULTS

In this section we present the results of photoconductivity measurements and discuss them in the light of the models described above. It is instructive in this process to start by developing a fuller characterization of the electron density of states, both in the bands and within the gap, as implied by the optical-absorption data in Fig. 1.

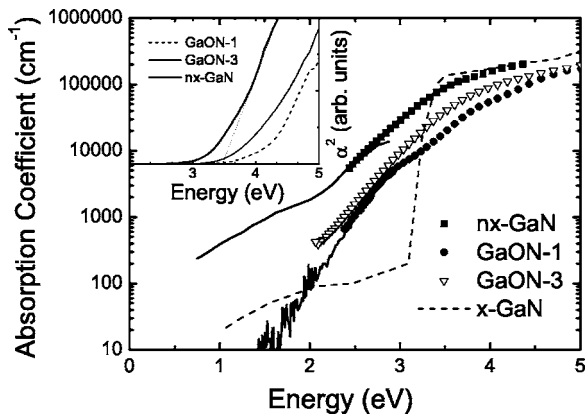


FIG. 1. Absorption coefficient determined from optical reflection and transmission (shown by symbols) as well as photothermal deflection (lines) for nc-GaN, GaON-1, and GaON-3. A crystalline GaN reference spectrum (*c*-GaN) is included for comparison. Inset: Square of absorption coefficient α vs energy, demonstrating the band-gap shift with increasing oxygen content.

A. Optical absorption and dark conductivity

As shown by the dashed line in Fig. 1, crystalline GaN (*c*-GaN) has an above-gap absorption coefficient α that is very close to that in our nc-GaN films, but with a very rapid drop to an impurity-determined level at energies below 3.4 eV. In the absence of such an unambiguous interband edge in our films it is necessary to estimate the mobility gap, separating valence- and conduction-band mobility edges, by an analysis appropriate for disordered materials. Previous work on nc-GaN (Refs. 16 and 17) has assumed an energy-dependent absorption appropriate for a direct-band-gap semiconductor, thus plotting α^2 versus energy and picking the gap from the extrapolated intercept. We have adopted this scheme for our nc-GaN films (see the inset to Fig. 1), which then are found to have a gap of 3.4 eV, almost the same as that found in *c*-GaN. This result contrasts with other reports which find blueshifting of the band gap in nanocrystalline GaN (Refs. 16 and 17) by this method. The blueshifting is associated in these other reports with the crystallite size becoming smaller than the calculated Bohr radius¹⁸ for excitons in *c*-GaN of 11 nm.

While the blueshifting of the band gap is not observed in the nc-GaN films grown by IAD, it is clearly seen in the amorphous GaON films. We have also plotted α^2 versus energy for these films in the inset to Fig. 1. Interestingly the shift is roughly proportional to the amount of oxygen in the films, indicating that oxygen incorporation at these high concentrations effectively changes the band structure of the material, and does not act as an impurity which introduces states in the gap. At this point we also note that not only is the gap wider in the oxynitrides but that the exponential tail of gap states is both lower and falls more rapidly into the gap; the tail of states extends much deeper into the center of the nc-GaN gap.

Having estimated the size of the gap between mobility edges, it is useful to determine the position of the Fermi level between them. To find it we turn to temperature-dependent measurements of the dark resistivities of the films. In all cases these follow an Arrhenius behavior as shown in Fig. 2, with activation energies in the range of 0.8–1.0 eV. These

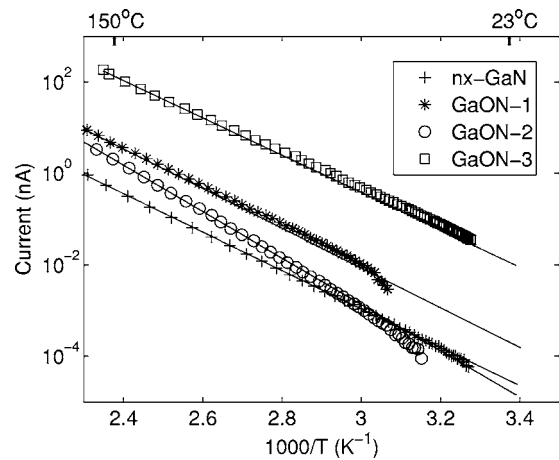


FIG. 2. Temperature dependence of dark conductivity for nc-GaN and GaON-1, -2, and -3.

values, corresponding to the positions of the Fermi level relative to the mobility edges, are consistent with the insulating nature of the samples at room temperature.

B. Photoconductivity

Now we may move on to investigate the photoconductivity. A strong distinction between the two classes of film is immediately observed in the time dependence of the photoresponse. Figure 3 shows the response under 300 nm illumination (overfilling the gap with an intensity of 10^{-5} W/cm²) for nc-GaN and *a*-GaON films. The nc-GaN film exhibits a weak photoconductivity (approximately 50 fA at 9 V, corresponding to 10^{-7} A/W) which is fast, switching on and off in times shorter than the 1 s resolution of this experiment. The GaON film, on the other hand, has a response several orders of magnitude greater (several nanoamperes at 9 V, corresponding to 10^{-2} A/W) which is very slow, decaying nonexponentially over the course of hours, i.e., showing PPC. The difference between the films is consistent with a barrier to recombination in the GaON films and no such barrier in the nc-GaN films.

This distinction observed in the time dependence was associated with similarly distinct characteristics of the steady-state photoconductivity described in the previous section. To see whether the description given there is consistent

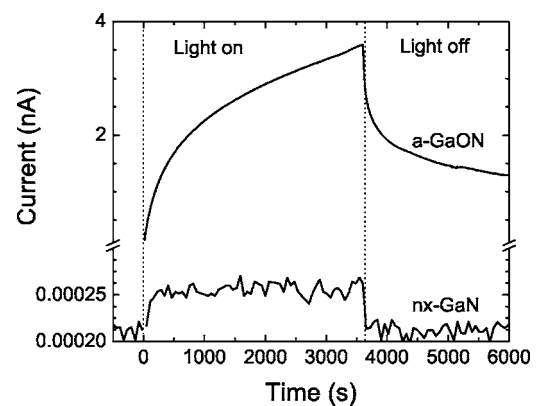


FIG. 3. Photoconductive response as a function of time for nc-GaN and *a*-GaON film.

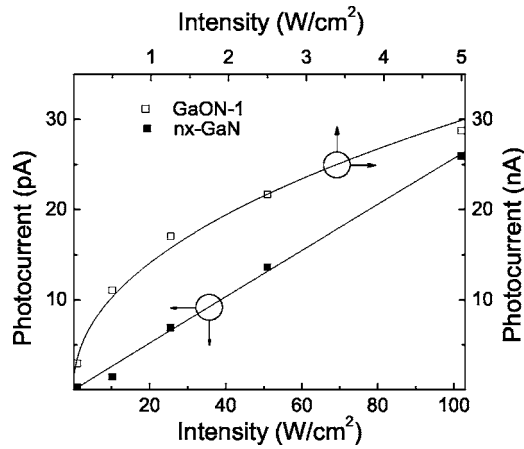


FIG. 4. Intensity dependence of photoconductivity in nc-GaN and GaON-1. The lines are power-law fits to the data.

with the films studied here, we now examine the generation rate dependence of the PC in the two classes of film. We can investigate this both by changing the absorption coefficient (by changing the wavelength) and by varying the intensity. The intensity dependence of the photoconductivity of the two films under the more intense laser source is shown in Fig. 4. A power-law fit to the GaON data gives an exponent of 0.46, and a fit to the nc-GaN data gives an exponent of 0.99. The exponents are very close to the 0.5 and 1 expected from films which do and do not exhibit PPC, respectively.

A second measure of the generation rate dependence of the PC is its dependence on absorption coefficient. The photoresponse, normalized by the incident power and then scaled for comparison with the absorption coefficient, is shown by symbols in Fig. 5 alongside the absorption coefficient (lines) for the films. The photoconductivity follows the absorption well, preserving the exponential drop-off in response with wavelength.

Remembering that the photoconductivity σ in the GaON films shows a square-root dependence on intensity I we com-

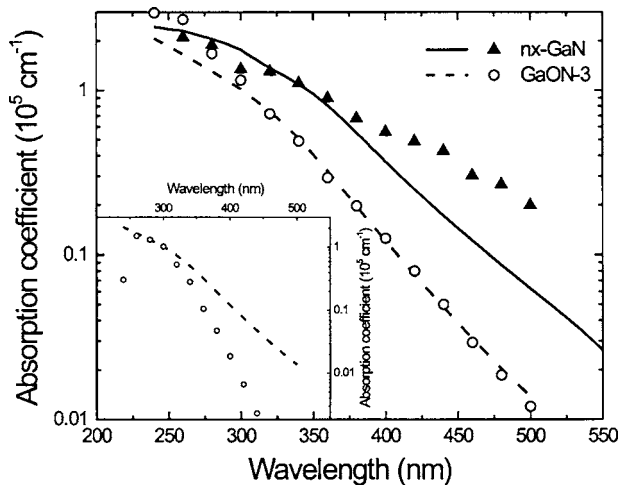


FIG. 5. Spectral dependence of the absorption coefficient (lines) and photoconductivity normalized to the incident intensity (symbols). Inset: photoconductivity data for GaON-3 normalized according to the square root of the incident intensity, consistent with the observed intensity dependence of the photoconductivity in this sample.

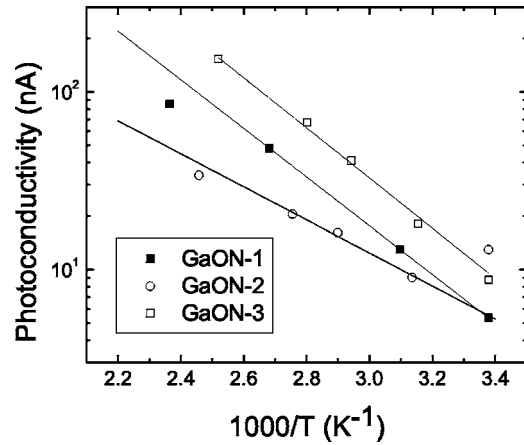


FIG. 6. Temperature dependence of the steady-state photoconductivity in GaON films.

pare σ^2/I (rather than σ/I) with the absorption coefficient in the inset to Fig. 5. The divergence from the expected behavior at long wavelengths may be related to the fact that the photoconductivity has not actually reached saturation after an hour of illumination (see Fig. 3). Our assumption that the films reach quasithermal equilibrium after this length of time is clearly an approximation and we must be careful in applying our model to this measurement.

Quasithermal equilibrium is, however, shown to be a good approximation when considering the temperature dependence of the steady-state PC in the GaON films. The magnitude of the PC response at different temperatures under 300 nm excitation is shown in Fig. 6 for the GaON films. In all cases it shows Arrhenius behavior, consistent with the predictions of our model based on the establishment of quasithermal equilibrium. The position of the quasi-Fermi-levels ($2E_f$) indicated by the curves for GaON-1, GaON-2, and GaON-3 are 0.5, 0.4, and 0.6 eV below the mobility edge, respectively. These values are consistent with the activation energies expected, i.e., the quasi-Fermi-level is shallower than the Fermi levels found for these materials.

C. Thermally stimulated conductivity

Annealing of the films at low temperatures proved to be very efficient at returning the films exhibiting PPC to a stable state. In addition, considerable information about the long-lived traps can be gleaned from the resulting thermally stimulated conductivity (TSC) curves produced during heating, which are shown for GaON-2 in Fig. 7.

The depth of the quasi-Fermi-level at the time we begin to heat the film is found by fitting an exponential function to the initial part of the curve as the film is heated.¹⁵ Since TSC curves were obtained after illumination of the films with different wavelengths and intensities, each curve corresponds to a different degree of filling of traps. The total density of occupied traps may also be found by integrating the area under the curve.¹⁵ Analysis of the different curves will therefore yield information about the density of occupied states at different depths below the mobility edge, and we can map out the density of states between the mobility edge and the Fermi level.

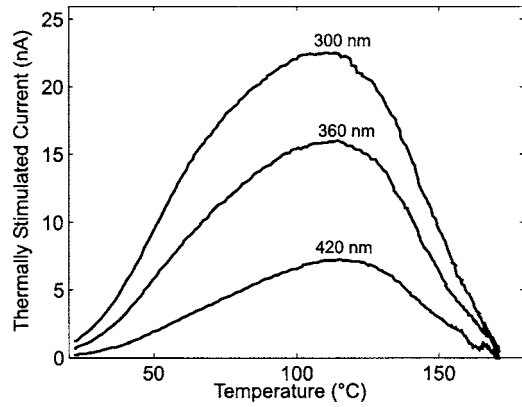


FIG. 7. Thermally stimulated conductivity curves for GaON-2 after illumination with different wavelengths.

We have taken the gain (number of electrons detected in external circuit per electron liberated from a trap) to be unity. The density determined in this manner is shown as a function of the quasi-Fermi-level as we begin heating in Fig. 8 for GaON-1 and GaON-3. The actual Fermi level obtained from the temperature dependence of the dark conductivity is also shown in the figure for the two films. This plot gives very clear evidence of an approximately exponential band tail above E_F with no significant deviations, consistent with the photothermal deflection curves shown in Fig. 1.

To check whether the gain of unity is reasonable, we have fitted an exponential to these data points and extrapolated toward the mobility edge. We find an integrated density of states at 0.1 eV below the mobility edge to be between 10^{23} and 10^{24} cm^{-3} . The number of atoms in the films is smaller than this, implying that the gain is larger than unity. For each electron freed from a trap during heating, more than one electron contribute to the current measured.

V. DISCUSSION

We will now proceed to build a picture of the density of states in the gap that contribute significantly to the photoconductivity. In so doing, the two classes of film can be distinguished and the origin of PPC can be postulated.

We know the position of the Fermi level from the temperature dependence of the dark conductivity. It is between

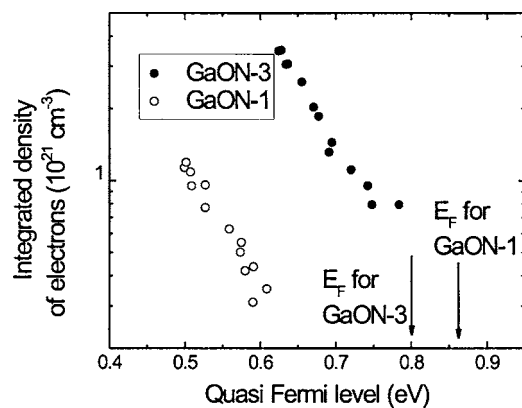


FIG. 8. Depth of quasi-Fermi-level vs density of ejected electrons found from TSC curves.

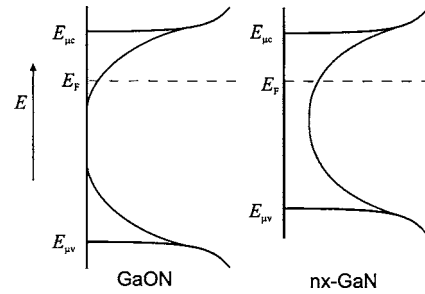


FIG. 9. Proposed density of states in GaON and nc-GaN films grown by IAD.

0.8 and 1 eV below the mobility edge for all of the films. Similar activation energies have been observed in other highly resistive disordered GaN. The microscopic origin is disputed but is generally attributed to native defect (vacancy and/or interstitial) complexes^{19,20} or grain-boundary states within a grain-boundary-controlled transport model.²¹

A high density of native defects is not unlikely in our material and any of these could be associated with the dominant activation energy. On the other hand, we have also found the distribution of localized states in the gap via spectral measurements: optical absorption, spectral photoconductivity, and TSC. All of these show only a smoothly varying density of states in the gap akin to exponential band tails. There is no evidence for a discrete level at which the Fermi level would be pinned. It is therefore more likely that the Fermi level simply lies somewhere within the band tails.

At this point we note a significant difference between the two classes of film insofar as the absorption coefficient is concerned. At low energies the absorption coefficient in the GaON continues to drop away sharply, while in the nc-GaN film there is a clear change in slope at these low energies (see Fig. 1). It seems that the density of states as we approach midgap is larger in the nc-GaN film than in the GaON films. This may account for the distinctions observed in the photoconductive behavior if the difference is enough to change the recombination path from being via thermalization in the nc-GaN to being via the extended states in the GaON films as the density of states at midgap is too low to support the cascading of carriers to the Fermi level.

Schematic representations of the implied densities of states are shown in Fig. 9. Note that we have once again chosen electrons to be the majority carrier. While it is true that unintentionally doped GaN is almost always *n* type, none of the measurements performed here allows us to actually distinguish whether this is the case in our films. However, if, in fact, holes are the majority carrier, all arguments may be reversed without altering the overall conclusions. In the GaON films we know that the mobility gap is larger than that of crystalline GaN and grows with the oxygen concentration in the film. X-ray emission spectroscopy measurements showed that the valence-band edges are displaced in energy⁸ so we have broadened the mobility gap by moving the valence band down in energy. In the nc-GaN film, the mobility gap is closer to that of crystalline GaN at 3.4 eV.

In the model for GaON, the origin of the PPC is the drop in the density of states at midgap as oxygen is introduced to

the film. The possibility that oxygen may act like a DX center (metastable donor which undergoes large lattice relaxation upon optical ionization) has been raised.^{22–24} However, the oxygen concentrations at which we observe PPC are at a level which induce significant structural and electronic changes in the material. Instead of simply introducing states in the gap (usually observed when impurities are incorporated into semiconductors at low concentrations), the oxygen alters the band structure, reducing the density of localized states relative to the nc-GaN as well as widening the gap between mobility edges. The effect of this on the photoconductivity is that recombination must now occur via extended states and PPC is observed. The model for photoconductivity which incorporates this concept describes almost all of the experimental observations we have made.

Finally, we comment on the likely utility of our material in visible-blind UV detectors. Using a simple photoresistor geometry and chopped light at 10 Hz we achieve a noise equivalent power of 10^{-8} W/ $\sqrt{\text{Hz}}$ under 300 nm illumination for the GaON films. This value is relatively high considering the fact that neither the material nor the detector geometry has been optimized at this stage, and thus GaON may indeed prove useful in UV detectors.

VI. CONCLUSIONS

In conclusion the experimental results described in this study have enabled us to characterize the optoelectronic behavior of nc-GaN and *a*-GaON grown by IAD. By analyzing the temperature dependence of the dark conductivity we found that the Fermi level lies about 1 eV away from the mobility edge. In the nc-GaN films, the photoresponse was fast but relatively weak, while the GaON films exhibited a much stronger, but persistent, photoconductivity. By examining the intensity dependence of the photoconductivity under 325 nm illumination the photoresponse was found to be linear in generation rate in the nc-GaN films and has a square-root dependence in the GaON films. Spectral dependence of the photoconductivity showed an exponential drop-off in the combined densities of states of the conduction- and valence-band tails with decreasing energy for both types of film. Analysis of TSC curves also revealed an exponential band tail of occupied states below the mobility edge and above the Fermi level in the GaON films. A gain greater than 1 in these films was implied by the analysis.

A model which considers the effect of a large density of localized states in the gap has been developed to describe the photoconductive behavior observed in these two types of film. If recombination of trapped carriers occurs via the conduction band, the characteristics observed in the GaON films are predicted. If direct recombination between trapped carriers is possible the characteristics exhibited by the nc-GaN films are expected.

ACKNOWLEDGMENTS

We gratefully acknowledge financial support from the New Zealand Foundation for Research Science and Technology through its New Economy Research Fund, and through doctoral (A.K.) and postdoctoral (B.J.R.) fellowships. We

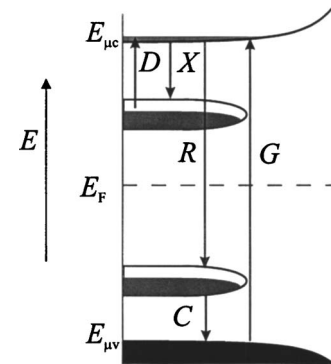


FIG. 10. Density of states and allowed transitions for semiconductor including hole and electron traps.

also thank Robert Kinsey at Canterbury University, Christchurch, New Zealand for making the interdigitated contacts to our films and John Kennedy at Geological and Nuclear Sciences, Lower Hutt, New Zealand for the RBS analysis of the films.

APPENDIX

In an effort to model the photoconductive behavior observed in the two classes of films studied in this work, the effect of large band tails of localized states on the steady-state photoconductivity was considered. Two classes were identified in the text, one in which the recombination takes place from the conduction band to a localized state and the other in which recombination occurs between localized carriers.

1. Recombination via extended states

We consider first the case in which recombination occurs via the conduction band. A schematic density of states, simplified to include only discrete levels of electron and hole traps, and the allowed transitions are shown in Fig. 10. G and R are the generation and recombination rates, X is the trapping rate, and D is the detrapping rate. The electron trap is distinguished from the hole trap by the fact that the electron detrapping time is short compared to the experiment time. The holes, on the other hand, are captured immediately and permanently by the hole traps via the transition marked C . The mobility edges of the conduction and valence bands are indicated as $E_{\mu c}$ and $E_{\mu v}$. We specifically exclude recombination between trap states.

We require two rate equations for n_c and n_t , the densities of excess electrons in extended states (conduction band) and in localized electron traps above the Fermi level, respectively. From Fig. 10 we can identify the transitions in and out of these states and can write

$$dn_c/dt = G - R - X + D,$$

$$dn_t/dt = X - D. \quad (\text{A1})$$

The recombination and trapping rates are proportional to the densities of carriers in the conduction band multiplied by

the density of recombination centers, ρ , and the density of unoccupied traps, $N_t - n_t$, respectively (N_t is the total density of traps).

Detrapping is a thermal process with activation energy E_t equal to the depth of the trap, so the detrapping rate will be proportional to $n_t \exp(-E_t/kT)$.

The second assumption we make is that the trapping/detrapping rates are larger than the recombination rate, resulting in quasithermal equilibrium between the free and trapped electrons. For this to be true, the number of unoccupied traps must be large (so that X remains large), i.e., $N_t \gg n_t$, so we can replace $N_t - n_t$ in the expression for X with N_t .

Under the two assumptions just discussed, the solution to Eq. (A1) becomes

$$n_c \propto \sqrt{G \exp(-E_t/kT)}. \quad (\text{A2})$$

The temperature dependence is explicitly included in Eq. (A2), with the photoconductivity varying with temperature as $\exp(-E_t/2kT)$ which follows from the quasithermal equilibrium condition. G is directly proportional to the light intensity so $n_c \sim I^{1/2}$ where I is the intensity of the incident light. G is also linear in absorption coefficient¹⁵ for $\alpha \lesssim 1/d$, and we have the same dependence of PC on absorption coefficient as on intensity, i.e., $n_c \sim \alpha^{1/2}$.

2. Recombination via localized states

Secondly we can contrast the above case with the case in which photogenerated holes cascade up from the valence band to the Fermi level as electrons thermalize down through localized states to the Fermi level and recombine with the holes trapped there.

In this case we may write for the steady state $G=R = n_c/\tau_r$ where τ_r is now the time of recombination via ther-

malization. For this recombination path τ_r is n_c independent so n_c will be linear in G and therefore also in I and in α .

- ¹S. Nakamura and G. Fasol, *The Blue Laser Diode* (Springer, Berlin, 1998).
- ²D. P. Bour, N. M. Nickel, C. G. V. de Walle, M. S. Kneissl, B. S. Krusor, P. Mei, and N. M. Johnson, *Appl. Phys. Lett.* **76**, 2182 (2000).
- ³P. Stumm and D. A. Drabold, *Phys. Rev. Lett.* **79**, 677 (1997).
- ⁴M. Yu and D. A. Drabold, *Solid State Commun.* **108**, 413 (1998).
- ⁵A. Bittar, H. J. Trodahl, N. T. Kemp, and A. Markwitz, *Appl. Phys. Lett.* **78**, 619 (2001).
- ⁶B. J. Ruck *et al.*, *Phys. Rev. B* **70**, 235202 (2004).
- ⁷F. Budde *et al.*, *J. Appl. Phys.* **98**, 063514 (2005).
- ⁸B. J. Ruck *et al.*, *J. Appl. Phys.* **96**, 3571 (2004).
- ⁹H. J. Trodahl, F. Budde, B. J. Ruck, S. Granville, A. Koo, and A. Bittar, *J. Appl. Phys.* **97**, 084309 (2005).
- ¹⁰W. B. Jackson, N. M. Amer, A. C. Boccara, and D. Fournier, *Appl. Opt.* **20**, 1333 (1981).
- ¹¹L. F. Lester, J. M. Brown, J. C. Ramer, L. Zhang, S. D. Hersee, and J. C. Zolper, *Appl. Phys. Lett.* **69**, 2737 (1996).
- ¹²M. E. Lin, Z. Ma, F. Y. Huang, Z. F. Fan, L. H. Allen, and H. Morkoc, *Appl. Phys. Lett.* **64**, 1003 (1994).
- ¹³B. P. Luther, S. E. Mohny, T. N. Jackson, M. A. Khan, Q. Chen, and J. W. Yang, *Appl. Phys. Lett.* **70**, 57 (1997).
- ¹⁴C. E. A. Grigorescu *et al.*, *Proceedings of 2003 Fifth International Conference on Transparent Optical Networks* (IEEE, New York, 2003), Vol. 1, p. 337.
- ¹⁵R. H. Bube, *Photoelectronic Properties of Semiconductors* (Cambridge University Press, Cambridge, 1992).
- ¹⁶N. Preshilla, S. Major, N. Kumar, I. Samajdar, and R. S. Srinivasa, *Appl. Phys. Lett.* **77**, 1861 (2000).
- ¹⁷J. W. Yoon, T. Sasaki, C. H. Roh, S. H. Shim, K. B. Shim, and N. Koshizaki, *Thin Solid Films* **471**, 273 (2004).
- ¹⁸Y. Xie, Y. Qian, W. Wang, and S. Zhang, *Science* **272**, 1926 (1996).
- ¹⁹S. J. Pearton, C. B. Vartuli, J. C. Zolper, C. Yuan, and R. A. Stall, *Appl. Phys. Lett.* **67**, 1435 (1995).
- ²⁰S. Kobayashi, S. Nonomura, T. Ohmori, K. Abe, S. Hirata, T. Uno, T. Gotoh, and S. Nitta, *Appl. Surf. Sci.* **113/114**, 480 (1997).
- ²¹J. Salzman, C. Uzan-Saguy, R. Kalish, V. Richter, and B. Meyler, *Appl. Phys. Lett.* **76**, 1431 (2000).
- ²²C. Wetzel *et al.*, *Phys. Rev. Lett.* **78**, 3923 (1997).
- ²³C. Wetzel, H. Amano, I. Akasaki, J. W. Ager III, I. Grzegory, B. K. Meyer, and M. Topf, *Phys. Rev. B* **61**, 8202 (2000).
- ²⁴C. G. V. de Walle, *Phys. Rev. B* **57**, R2033 (1998).